Journal of Computing and Electronic Information Management
ISSN: 2413-1660 | Vol. 20, No. 1, 2026

Numerical Simulation Study on the Holding Force and Pull-out Strength of Surface-Set Diamond Core Bits

Jingcheng Li, Yang Li, Jiahao Wang, Zhi Yang

School of Mechatronic Engineering, Southwest Petroleum University, Chengdu 610500, China

Abstract: To investigate the gripping force characteristics of surface-mounted single-grain diamonds and their detachment behavior under complex loading conditions, this study combines finite element numerical simulation and experimental verification to establish a three-dimensional mechanical model of the "metal matrix–interface–diamond" system. The distribution and evolution of the gripping force under the coupled effects of multiple factors, including diamond particle shape, size, exposure height, and inclination angle, are systematically analyzed. The results indicate that: (1) The topological structure of regular polyhedral abrasive particles determines their interfacial retention performance. Specifically, the dodecahedron exhibits the highest bonding strength, while the hexahedron shows the best energy absorption capacity. (2) Reducing the exposure height of abrasive particles significantly enhances both the interfacial retention force and toughness, which is a key factor in optimizing retention performance. (3) The interfacial retention performance is positively correlated with diamond particle size; larger particles can synergistically improve both the strength and toughness of the tool interface. (4) Inclined implantation of diamond particles can effectively regulate retention performance: a 45°inclination corresponds to the highest tensile strength, while a 30°inclination provides the best impact toughness.

Keywords: Surface Set Diamond Bit; Single diamond particle; Control power; Range analysis.

1. Introduction

With the extension of exploration and development to deep strata and unconventional oil and gas reservoirs[1–3], the importance of coring technology has become more and more prominent, and its core value lies in the ability to obtain the original samples of underground rock formations in a complete manner. By directly obtaining the real stratum cores, it provides irreplaceable first-hand information for geological research, mineral and oil and gas reservoir evaluation and engineering decision-making[4–7].

Conventional PDC core drill bit mainly relies on the shearing effect of cutting teeth to break the formation[8,9]. For hard, fractured formations exhibiting poor drillability, high abrasion resistance, and extensively developed fractures, conventional PDC coring bits are susceptible to unstable loading, imbalanced cutting actions, and severe longitudinal and transverse vibrations. These conditions readily lead to the fracturing or dislodgement of the primary cutting teeth, thereby accelerating wear on the remaining teeth and the bit body.[10–13].

Surface mounted diamond drill bits are widely used due to the wear resistance of their cutting elements, good impact toughness, superior cutting efficiency, and high adaptability[14–16]. During the rock-breaking process of surface-mounted diamond drill bits, diamond particles are subjected to severe impact, high-stress shear, and continuous frictional wear from the rock. The main failure modes include dulling, fragmentation, and detachment. Among these, the premature detachment of diamond particles not only results in the unexpected loss of costly materials but also leads to an irreversible decline in the cutting ability of the drill bit. This represents a primary bottleneck restricting both the service life and drilling economy of the bit. The fundamental cause of this failure behavior lies in the insufficient "gripping force" exerted by the metal powder metallurgy matrix on the diamond particles. Therefore, systematically revealing the formation mechanism, evolution law, and failure criteria of the gripping force from a mechanical perspective provides the theoretical basis for achieving structural optimization, performance prediction, and lifespan extension of the drill bit.

At present, scholars at home and abroad have conducted extensive research on the control mechanism of diamond tools, mainly focusing on two aspects: firstly, by changing the matrix formula (such as adding carbide forming elements[17–20], rare earth elements[21–24], etc.) or using surface coating[25–29], etching[30,31] and other pretreatment processes to enhance the chemical metallurgical bonding and mechanical meshing between diamond and matrix; The second is to evaluate the overall encapsulation performance of the tire body through macroscopic mechanical experiments (such as bending[20] and impact tests) or simplified models. However, existing research mostly focuses on material modification or macroscopic performance testing. There is still a lack of systematic and quantitative analysis on the intrinsic correlation mechanism between the geometric characteristics (such as shape, particle size, exposure height, implantation angle) and interface mechanical behavior of single diamond particles under complex stress states. Especially, numerical simulation of the interface failure process under the coupling of multiple factors is still insufficient.

In response to the issues described above, this study addresses the fundamental cause of the macroscopic detachment of individual diamond particles in surface-mounted diamond drill bits—the gripping force provided by the matrix. A research methodology combining finite-element numerical simulation and experimental verification is adopted. First, a three-dimensional mechanical model of the "metal matrix–interface–diamond" system is established to simulate the interfacial failure process of diamond under tensile loading. This model is used to systematically investigate the influence of multiple factors—such as diamond shape, particle size, exposure height, and inclination

angle—on the interfacial bond strength and failure behavior. Second, based on the numerical simulation results, range analysis is employed to quantify the relative importance of each factor on the gripping force. Finally, three-point bending tests are conducted to measure the bending strength of matrix samples containing diamonds of different particle sizes and exposure heights, thereby validating and supplementing the numerical simulation conclusions from the perspective of macroscopic mechanical properties. This study aims to reveal the key factors influencing the gripping failure of surface-mounted single diamond particles from both micro-mechanical mechanisms and macro-performance perspectives, thereby providing a theoretical basis and data support for the structural optimization and performance enhancement of diamond drill bits.

2. Simulation methodology

The "abnormal detachment" of diamonds is the primary cause of diamond drill bit failure, which manifests as the failure of the bonding interface between the metal matrix and the diamond, leading to the detachment of diamond particles. When diamond particles detach, the cracks that form at their bonding interface are generally classified by researchers into three fundamental fracture modes: pure Mode I (opening mode), pure Mode II (sliding mode), and pure Mode III (tearing mode). These three fracture types are illustrated in Figure 1. In the opening mode (Mode I), the normal stress acts perpendicular to the crack surface, and the crack propagates perpendicular to its front. In the sliding mode (Mode II), the shear stress is parallel to both the crack plane and the direction of crack propagation. In the tearing mode (Mode III), the shear stress is perpendicular to the direction of crack propagation. Given the complex characteristics of the interface between diamond particles and the metal matrix, mixed fracture modes may occur at the matrix–diamond interface. Therefore, it is assumed that all three aforementioned fracture modes can be present.

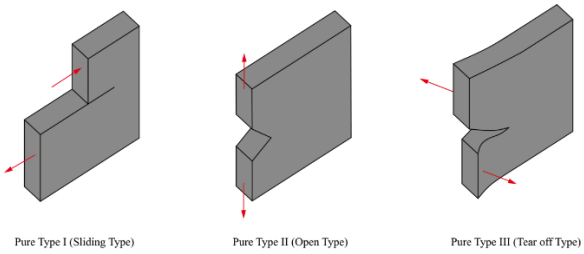

Figure 1. Schematic diagram of three types of fracture forms

When studying the interface behavior between diamond tools and diamond, researchers considered that cracks and debonding phenomena may occur at the interface when diamond is loaded and detached. They proposed three finite element simulation models based on the interface behavior between metal matrix and diamond, namely the birth and death element model, the elastic layer element model, and the cohesive force element model[32–34]. Considering that the cohesive zone model (CZM) can accurately describe the entire process of interfacial deformation from elasticity to failure, and simulate crack initiation, propagation, and debonding behavior through a traction-separation law—thereby avoiding the stress singularity problem inherent in traditional fracture mechanics—this approach is well-suited to the present study. Therefore, the cohesive zone model is employed to simulate the interface behavior between the metal-based matrix and the diamond. Common criteria for determining the onset of crack initiation include quadratic stress criterion, maximum stress criterion, quadratic strain criterion, maximum strain criterion, among others. In mixed failure mode, the secondary failure criterion proposed by Cui[35] is used to predict the initiation of cracks, and its expression is:

$$\left\{\frac{\varepsilon_n}{\varepsilon_n^o}\right\}^2+\left\{\frac{\varepsilon_s}{\varepsilon_s^o}\right\}^2+\left\{\frac{\varepsilon_t}{\varepsilon_t^o}\right\}^2=1$$

where, ε_n, ε_s, ε_t represent the normal stress and tangential stress of the element mesh, respectively, ε_n^o, ε_s^o, ε_t^o respectively represent the stress intensity in the normal and tangential directions.

The most commonly used constitutive model for the traction separation law is the bilinear constitutive model, which can effectively calculate the accuracy and efficiency of the model. The bilinear constitutive model is shown in Figure 2.

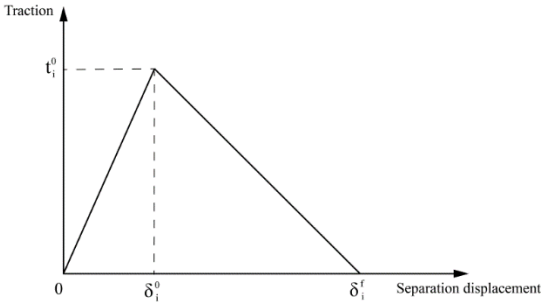

Figure 2. Bilinear elastic fracture constitutive model

When establishing a cohesive element model, a cohesive layer needs to be defined between the diamond particles and the matrix. Cohesive layers typically exist in two forms: a thick cohesive layer and a zero-thickness cohesive layer. Given that modeling a thick cohesive layer requires the separate creation of geometric entities, and considering the variable shapes of diamond particles which would further complicate the model geometry, constructing thick cohesive elements individually between the diamond particles and the matrix is excessively intricate. In contrast, the zero-thickness cohesive layer is implemented by sharing nodes between the matrix and the diamond to form cohesive elements, which is both simpler and more physically realistic. In this study, the zero-thickness cohesive layer is used to characterize the interfacial behavior between the matrix and the diamond, as illustrated in Figure 3.

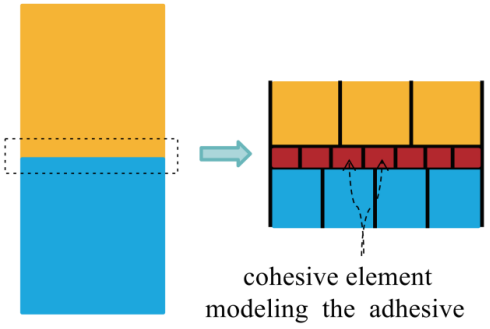

Figure 3. Schematic diagram of cohesive unit layer

3. Numerical simulation of single diamond particle holding force

3.1. Base case

In this study, the interfacial characteristics between diamond particles and the metal matrix in diamond drill bits were investigated using a commonly adopted single-diamond abrasive model. The geometric model consists of two parts: the metal matrix and the diamond particle. To mitigate stress concentrations caused by geometric discontinuities in finite element analysis, a cylindrical shape was adopted for the metal matrix, while five representative particle geometries were selected: the regular octahedron, truncated octahedron, regular hexahedron, regular dodecahedron, and regular icosahedron. Given its brittle nature, diamond was modeled as an isotropic linear elastic material. A hard alloy, specifically tungsten carbide–cobalt (WC–8Co), was employed as the metal-matrix material due to its high wear resistance, substantial hardness, and strong adhesive properties.[36]. The mixed mode constitutive equation of cohesive interface is defined by four material properties by assuming that the toughness and strength in the two tangential directions of the model are equal to each other: ε_n^o, ε_s^o, G_{IC}, G_{IIC} [37].Due to the lack of available experimental methods to directly determine the interface parameters of diamond drill bits, and the fact that the exact values of interface characteristics are not necessary for this study, the material properties of the matrix are used as interface material parameters.

The diamond is embedded at the center of the metal matrix, leaving a specified protrusion height. The contact interface between the diamond particle and the metal matrix is defined as a cohesive layer to simulate interfacial behavior. Mesh refinement is applied around the cohesive layer, with the diamond and the cohesive layer sharing the same seed density. This ensures accurate transmission of interfacial mechanical behavior and enables a realistic simulation of damage evolution. Both the diamond and the metal-matrix components are discretized using 4-node linear tetrahedral (C3D4) elements with linear pressure formulation. The total number of elements in the metal-matrix body is 110665. The cohesive layer is introduced using inserted cohesive seams, and its mesh type is COH3D6—a four-node three-dimensional cohesive element, as illustrated in Figure 4.

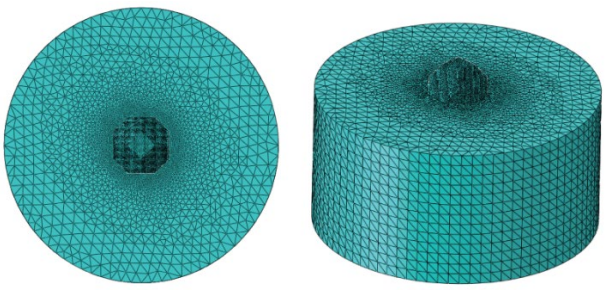

Figure 4. Mesh discretization diagram

The boundary conditions and loading setup are illustrated in Figure 5. Contact between the diamond and the cohesive layer is defined as surface-to-surface contact, with a friction coefficient set to 0.1. Loading is applied by imposing a constant horizontal velocity of 0.1 m/s at the tip of the diamond while all six degrees of freedom at the bottom of the metal substrate are fixed. Under quasi-static loading conditions, the detachment behavior of diamond particles can be systematically examined by extracting the load-time response curve at the loading point. As the displacement-controlled load progresses, interface damage initiates and propagates when the interfacial stress reaches and exceeds the critical bond strength of the cohesive layer. This critical state corresponds to the first peak in the load-displacement curve, marking the onset of diamond particle detachment. The peak load quantitatively characterizes the interfacial adhesion strength, while the corresponding displacement reflects the overall deformation capability of the material system. The subsequent descending portion of the curve represents the gradual evolution of interfacial damage.

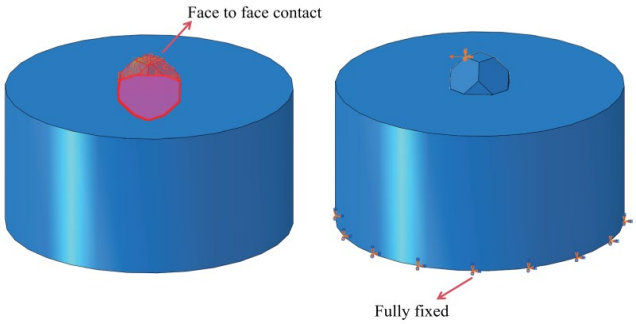

Figure 5. Boundary conditions and load settings

Table 1. Characteristic parameters of diamond, matrix and interface materials

Type		Diamond	WC-8%Co	Cohesive
Young's Modulus (Gpa)		1100	600	600
Poisson's Ratio		0.2	0.22	0.22
Density (g/cm^3)		350	14.5	14.5
Johnson-Cook Plasticity	A(Mpa)	-	4050	-
	B(Mpa)	-	1050	-
	n	-	0.21	-
	m	-	1.0	-
Quade Damage	ε_n^o (Mpa)	-	-	543
	ε_s^o, ε_t^o (Mpa)	-	-	314
	G_{IC} (mJ/mm^2)	-	-	0.14
	G_{IIC}, G_{IIIC} (mJ/mm^2)	-	-	0.33

3.2. Numerical simulation scheme

Table 2. Numerical simulation scheme table for diamond holding force

No.	Influencing Factor	Shape	Size (mm)	Protrusion Height (mm)	Orientation (°)
1	Shape	Regular Octahedron	1.6	0.8	0
2		Truncated Octahedron			
3		Cube			
4		Regular Dodecahedron			
5		Regular Icosahedron			
6	Particle Size	Regular Octahedron	0.8	0.5	0
7			1.2		
8			1.6		
9			2.0		
10			2.4		
11	Protrusion Height	Cube	1.6	0.4	0
12				0.5	
13				0.6	
14				0.7	
15				0.8	
16	Orientation	Truncated Octahedron	1.6	0.8	0
17					15
18					30
19					45
20					60

4. Analysis of Impact Results

4.1. Effect of abrasive grain shape

The shape of abrasive particles significantly influences the clamping force exerted by the metal-based matrix on the diamond. Due to differences in parameters such as sharpness, number of edges, and edge size, abrasive particles exhibit varying levels of retention within the metal-based matrix. Figure 6 illustrates different forms of natural diamonds, which occur in diverse morphologies. Single crystals can be categorized into cubes, octahedra, truncated octahedron, rhombic dodecahedra, as well as convex dodecahedra, convex hexahedra, and their aggregates. Aggregates are more commonly observed than single crystals with regular geometric shapes.

Figure 6. Different Natural Diamond Shapes Diagram

Referring to the shape of natural diamond, regular octahedra, truncated octahedra, regular hexahedron, regular dodecahedron, and regular icosahedron were selected as the objects of this study to investigate the influence of diamond shape on grip force. (Figure 7)

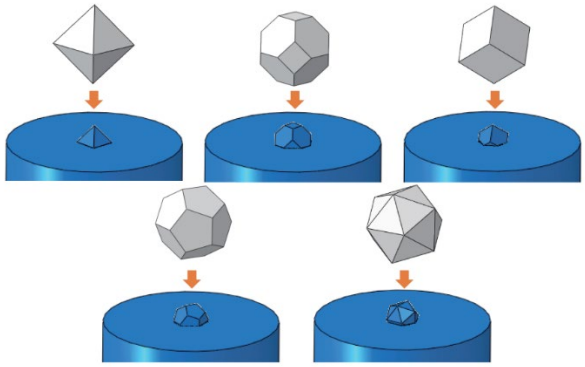

Figure 7. Diagram of the interaction between abrasive particles of different shapes and the matrix

There is a significant coupling effect between the geometric morphology of diamond particles and their retention strength within the matrix. Specifically, variations in morphological features—such as edge sharpness, crystal plane orientation, and surface texture—can lead to substantially different interfacial mechanical responses, thereby affecting the retention strength. The load time curves extracted from the loading points for different abrasive-particle shapes are presented in Figure 8. As shown, regular dodecahedral diamond particles exhibit the highest retention capacity due to their stronger interfacial adhesion, with a peak force of approximately 963.82 N, followed by the regular icosahedron (801.98 N) and the regular hexahedron (575.75 N). The critical interface-debonding forces for the regular octahedron and the truncated octahedron are similar, measuring 382.73 N and 338.79 N, respectively. Among the five diamond shapes, only the regular hexahedron displays a stepped decay after reaching its peak force in the elastic stage, eventually declining to zero load-bearing capacity. The other four shapes show a slight initial decrease after the peak, followed by a continued increase. This behavior is attributed to mechanical interlocking between the diamond particles and the metal matrix after interfacial debonding, which helps retain the diamond in the matrix instead of allowing immediate detachment. Figure 9 illustrates the first-peak

force and the corresponding work curves for different abrasive-particle shapes. It can be observed that the regular hexahedral diamond abrasive particle consumes the highest amount of work at the first peak. This is because its six flat surfaces provide a large contact area with the matrix and a strong initial bond. However, its sharp 90° edges generate high stress concentrations under loading, inducing early cracking in the matrix and absorbing considerable energy, which explains the highest associated work. In contrast, the truncated octahedron exhibits the least work at the first peak. Its shape removes the most effective mechanical anchoring points, approximating a sphere. The smooth geometry makes it difficult to develop significant stress concentrations in the matrix under load, rendering it more susceptible to interfacial debonding.

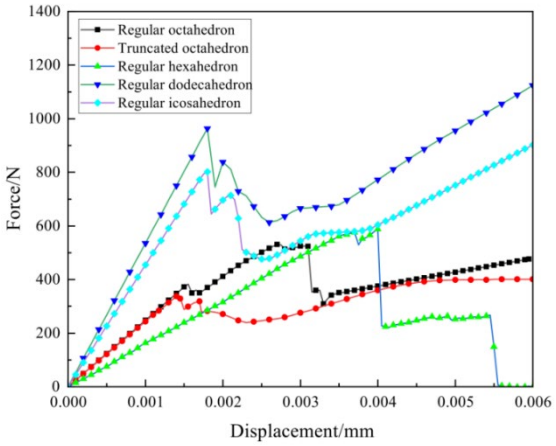

Figure 8. Reaction force time curves of loading points extracted from abrasive particles of different shapes

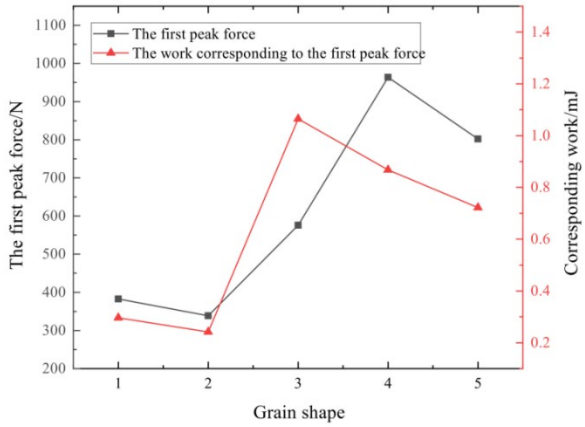

Figure 9. The first peak force and its corresponding work curve under different abrasive particle shapes (in the x-axis coordinates of the figure, 1-5 are: regular octahedron, truncated octahedron, regular hexahedron, regular dodecahedron, regular icosahedron)

4.2. Effect of abrasive grain size

Among the many factors influencing gripping performance, diamond particle size is a key variable. Significant differences exist in the distribution, interfacial bonding area, and stress characteristics of diamond particles of different sizes within the matrix. Table 3 lists the diamond particle sizes commonly used in surface-mounted drill bits, with two size ranges selected for this study: ultra-coarse and coarse. To ensure that the modeling of abrasive particle size meets the research requirements, the geometry was accurately represented based on the circumscribed-sphere radius formula for regular polyhedrons, where the parameter "a" denotes the edge length of the geometric model of the abrasive particle.

Table 3. Diamond particle size used for surface mounted drill bits

GPA	Coarse Grain	Medium Grain	Fine Grain	Extra Fine Grain	Ultra-fine Grain
Size Range (mm)	8~15	15~25	25~40	40~60	60~100
Korean Standard	Soft to Medium Hard	Medium Hard	Hard	Hard to Hardest	Hardest
Size Range (mm)	1.2~2.0	0.71~1.2	0.425~0.71	0.25~0.425	0.15~0.25

Table 4. Theoretical formula table for the outer diameter of diamond particles with different shapes

Diamond Shape	Cube	Truncated Octahedron	Regular Octahedron	Regular Dodecahedron	Regular Icosahedron
Circumscribed Sphere Diameter	$\frac{\sqrt{3}a}{2}$	-	$\frac{\sqrt{2}a}{2}$	$\frac{\sqrt{3}+\sqrt{15}a}{4}$	$\frac{\sqrt{10+2\sqrt{5}a}}{4}$

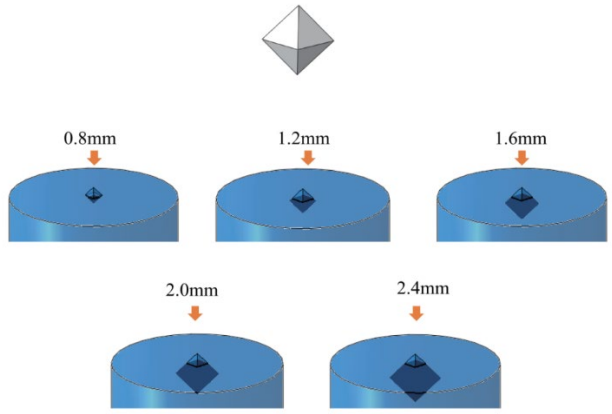

Figure 10. Diagram of the interaction between abrasive particles of different sizes and the matrix

The response characteristics of diamond holding force with respect to particle size variation represent a core criterion for characterizing the mechanical behavior of the matrix-diamond interface. The load-time curves extracted at the loading points for different particle sizes are shown in Figure 10. As observed, the force-time trends for different particle sizes are largely similar: as displacement loading proceeds, the force curve gradually rises, reaches a first peak, then gradually declines, stabilizes at a certain level, and subsequently exhibits a minor increase. Figure 11 presents the first-peak force and its corresponding work curve for different abrasive particle sizes. The results indicate a strong positive correlation between particle size and interfacial retention performance (peak force and work). This correlation arises because, at the same exposure height, larger particle sizes correspond to greater surface area and volume of matrix material embedded with the abrasive particles. The increase in particle size from 1.6 mm to 2.0 mm represents a key turning point: the peak force rises from 553.96 N to 1107.84 N, and the corresponding work increases from 0.94 mJ to 2.63 mJ. Both the peak force and the work approximately

double within this range, demonstrating that the effect of increasing particle size on gripping performance is highly significant. Increasing the particle size enlarges the "foundation" portion embedded within the matrix, which effectively enhances resistance to bending moments, distributes stress over a larger interfacial area, and helps avoid early failure due to localized stress concentration. At a particle size of 2.4 mm, both the first-peak force and the corresponding work reach their maximum values, indicating that larger abrasive particles can more effectively dissipate energy and suppress the rapid initiation and propagation of cracks. This behavior is crucial for improving the impact toughness of the tool. (Figure 12)

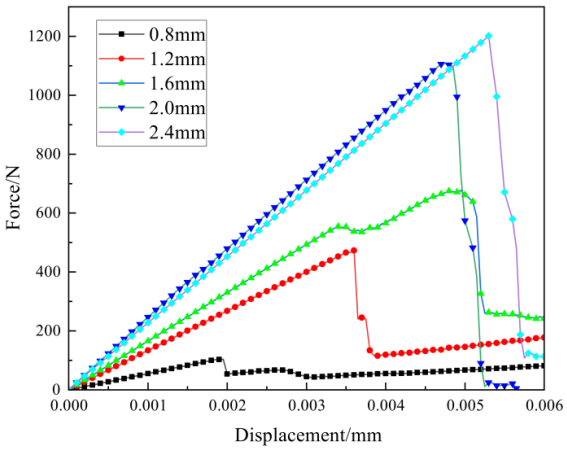

Figure 11. Reaction force time curves of loading points extracted from different particle sizes

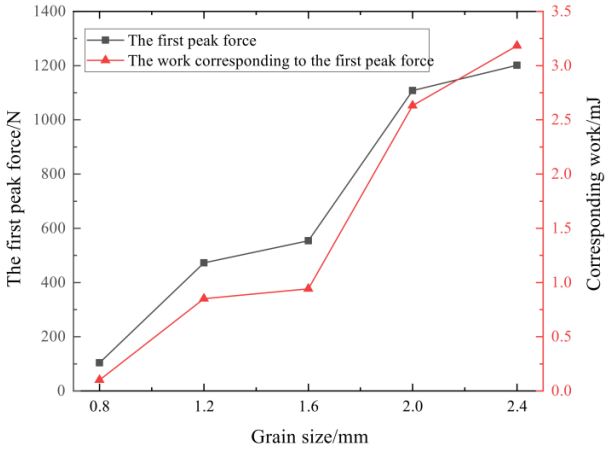

Figure 12. The first peak force and its corresponding work curve under different abrasive particle sizes

4.3. Effect of abrasive grain exposure height

The gripping force exerted on abrasive grains is closely related to the protrusion height of the grains. Due to the shared contact interface between diamond abrasive grains and the metal matrix, both the number and orientation of grains embedded in the matrix vary with changes in the diamond protrusion height. Consequently, the gripping force applied to the abrasive grains also changes with protrusion height. A schematic of the diamond particle protrusion height is shown in Figure 13. The protrusion height is defined as the vertical distance from the highest point of the exposed portion of the diamond to the nearest end face of the matrix body.

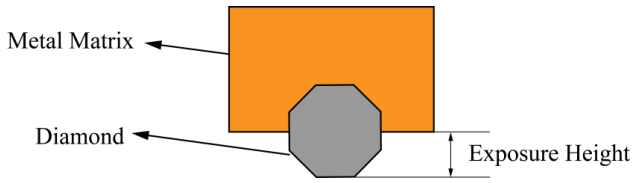

Figure 13. Schematic diagram of diamond particle exposure height

Select a 1.6mm particle size regular hexahedral diamond as a model to explore the influence of different exposure heights. (Figure 14)

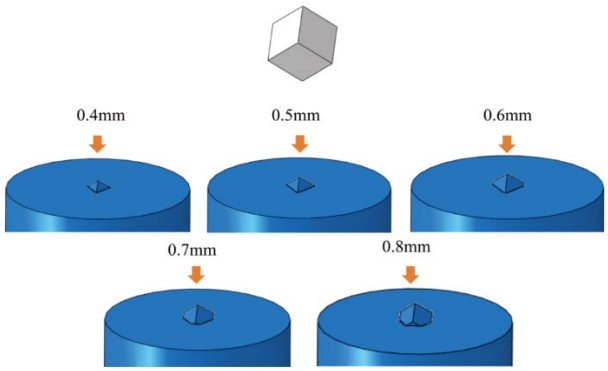

Figure 14. Diagram of the interaction between abrasive particles and matrix at different exposure heights

The relationship between diamond holding force and exposure height reveals key mechanical characteristics of the interfacial bonding performance. Figure 15 shows the load–time curves extracted at the loading points for different exposure heights. As observed, the force–time trends for the regular hexahedral diamond are largely similar across different exposure heights: after reaching the first peak force, the curves undergo a stepwise decay and eventually drop to zero, indicating complete debonding failure. Figure 16 presents the first-peak force and its corresponding work for various exposure heights. The results show that at the lowest exposure height of 0.4 mm, the first-peak force is highest (1107.22 N) and the corresponding work is also maximal (1.77 mJ). This is because most of the diamond abrasive particle is firmly embedded within the matrix material, providing the largest contact area and strongest mechanical interlocking. As the diamond exposure height increases, the first-peak force decreases non-linearly. When the height increases from 0.4 mm to 0.5 mm, the first-peak force drops sharply from 1107.22 N to 673.95 N—a reduction of 39.2%—primarily due to the decrease in effective load-bearing area. According to Hertzs [38] contact theory, it can be inferred that the effective bearing area decreases quadratically with increasing exposure height. As the ratio of exposure height to particle size increases from 0.25 to 0.3125, the edges and corners of the diamond become progressively more exposed. Consequently, the embedding capability of the metal-based matrix diminishes, and the bending moment induced by the applied load during exposure-height increase generates high tensile and shear stress concentrations at the root of the abrasive-matrix joint. This leads to a relatively low overall load-carrying capacity. The matrix undergoes local fracture or rapid crack propagation, causing the diamond particles to be "levered out". Within the exposure-height range of 0.5 mm to 0.8 mm, the reduction in the first-peak force is much smaller than that observed when the height increased from 0.4 mm to 0.5 mm, with a maximum decrease of only 9.4%. A slight increase even occurs between 0.7 mm and 0.8 mm, which

may be attributed to stress redistribution resulting from localized plastic strain or enhanced mechanical interlocking, leading to increased adhesive strength in the most critical region.

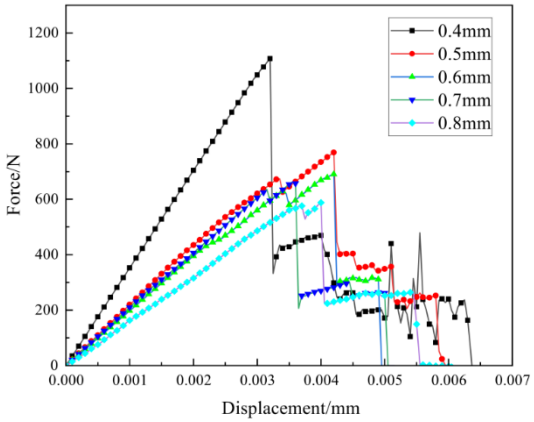

Figure 15. Reaction force time curves of loading points extracted from different exposure heights

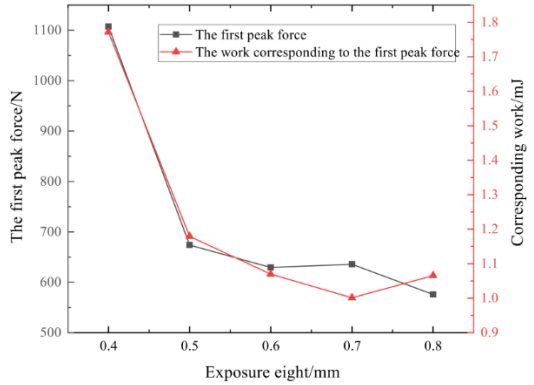

Figure 16. The first peak force and its corresponding work curve at different exposure heights

4.4. Effect of abrasive grain posture

Due to the fact that diamond particles are not perfectly spherical but possess distinct edges and corners, and because their positioning on the metal matrix during processing is not completely uniform, a variety of orientations and angles can occur. As a result, the gripping force exerted on the abrasive particles also varies with their posture. In this study, the influence of diamond inclination angle on gripping performance is examined sequentially at 0°, 15°, 30°, 45°, and 60°, where 0° corresponds to a vertically oriented diamond, as illustrated in Figure 17 & 18.

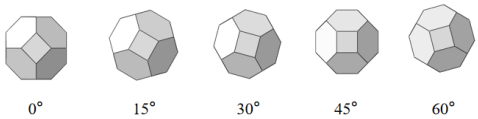

Figure 17. Model diagrams of diamond particles in different poses (from left to right: 0 °, 15 °, 30 °, 45 °, 60 °)

The spatial orientation of diamond particles is a key geometric parameter influencing interfacial gripping performance. The load–time curves extracted at the loading points for different orientations are shown in Figure 19. As observed, at inclination angles of 15° and 45°, the force increases to a first peak, then declines slightly before rising again. At 0°, the force decreases moderately after the peak and then undergoes a stepwise decay after reaching a certain level. At 30° and 60°, the applied force decreases after the peak and subsequently stabilizes. This stabilization indicates a fundamental change in the failure mechanism: the diamond particle no longer engages in mechanical interlocking with the matrix but instead acts like a plow, with its sharp edges continuously scraping and ploughing through the matrix material. Figure 20 presents the corresponding critical separation forces for different orientations. It can be seen that the critical separation forces at 15° (1436.76 N) and 45° (1466.70 N) are similar, with the highest value occurring at 45°. This means that when the diamond is inclined at 15° or 45° within the matrix, a larger force is required to separate the diamond–matrix interface in the push-shear test. The critical forces at 30° (921.31 N) and 60° (926.20 N) are also comparable, which can be attributed to the symmetrical geometry of the truncated octahedron; at the same exposure height, the degree of diamond encapsulation by the matrix is not significantly different between these two angles. At the minimum inclination of 0°, the critical force is 508.91 N—approximately three times lower than the maximum value—demonstrating that diamond inclination is a significant factor affecting the interfacial separation strength. Although the peak force at 30° is lower than that at 15° and 45°, the work consumed is higher. This is because the failure mode transitions from brittle fracture to ductile slip and plastic ploughing, allowing more energy to be absorbed over a longer failure displacement.

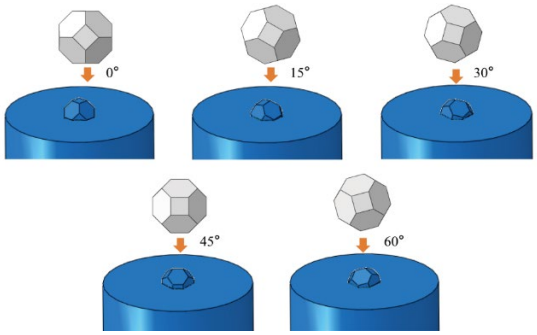

Figure 18. Interaction diagram between abrasive particles and matrix in different poses

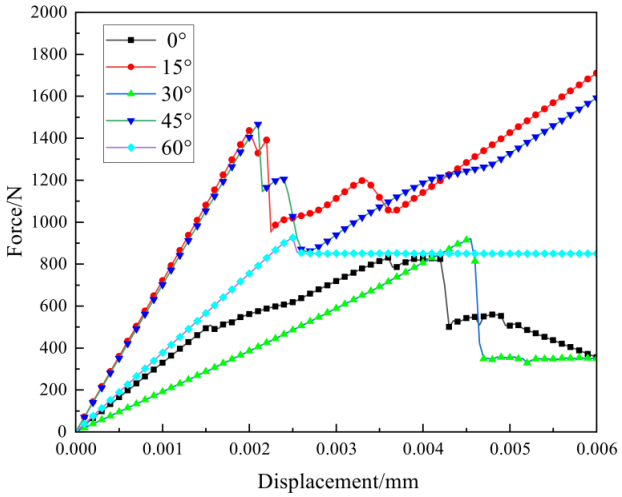

Figure 19. Reaction force time curve of loading points extracted from different poses

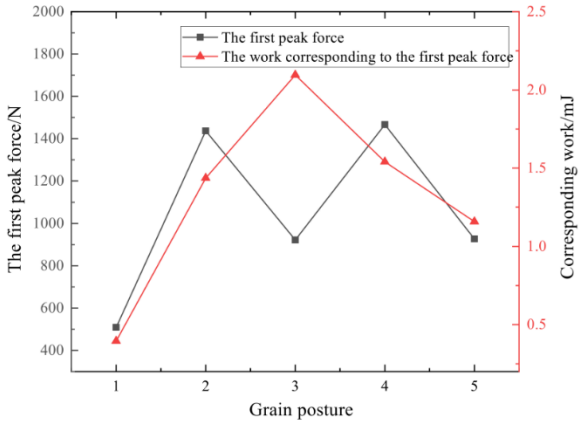

Figure 20. The first peak force and its corresponding work curve under different poses (in the x-axis coordinates of the figure, 1-5 are: 0 °, 15 °, 30 °, 45 °, 60 °)

5. Conclusion

This study establishes a three-dimensional numerical simulation model of a "metal-matrix–interface–diamond-particle" system. By integrating elastoplastic mechanics theory with the cohesive zone model (CZM), and employing a push-shear method, it explores multiple key factors affecting the interfacial behavior of a single diamond particle in the matrix—including its geometric shape, particle size, exposure height, and spatial orientation. The aim is to systematically examine how these factors jointly influence the interfacial bonding performance and gripping strength between the matrix and the diamond, thereby revealing the mechanical mechanisms underlying interface bonding in diamond tools. The work provides quantitative theoretical insights and a simulation-based foundation for the structural optimization, interface modification, and strength-enhancement design of high-performance diamond tools. The main conclusions are as follows:

(1) The gripping performance of regular polyhedral abrasive particles is closely related to their topological characteristics. The number and sharpness of vertices and edges are the core factors determining the grip strength, while the shape and orientation of the faces jointly influence the failure modes and energy absorption. Regular dodecahedral abrasive particles exhibit the highest interfacial bonding strength, which is attributed to the superior mechanical interlocking effect resulting from their maximum number of vertices. In contrast, regular hexahedral abrasive particles show the best energy dissipation capacity; the complex crack propagation paths induced by their sharp edges significantly increase the energy consumed during interfacial fracture. For the design of diamond drill-bit matrices, regular dodecahedral particles should be preferred if ultimate tensile strength is the primary objective, whereas regular hexahedral particles are a better choice when impact toughness and energy absorption need to be improved.

(2) Exposure height has a significant negative influence on interfacial gripping performance. Numerical simulations indicate that when the exposure height increases from 0.4 mm to 0.8 mm, the peak gripping force at the interface decreases by about 48% (from 1107 N to 576 N), and the failure energy decreases by about 40% (from 1.77 mJ to 1.07 mJ). This confirms that the strong mechanical interlocking provided by a low exposure height is key to optimizing gripping performance. A lower diamond exposure height effectively suppresses bending-moment effects during pull-out by maximizing the volume of matrix surrounding the particle, promoting ductile tearing rather than brittle fracture at the interface and thereby enhancing both bonding strength and toughness simultaneously.

(3) Diamond particle size is one of the most critical geometric parameters governing interfacial holding performance. Within the range of 0.8 mm to 2.4 mm, the peak gripping force and failure energy at the interface show an almost monotonic and significant increase with increasing particle size. The bonding strength (1201 N) and energy-dissipation capacity of abrasive particles with a size of 2.4 mm reach about 11.6 times and 31.8 times those of 0.8 mm particles, respectively. This is primarily attributed to the larger mechanical interlocking area and the extended crack-propagation energy-dissipation path provided by larger particles. These results reveal the considerable potential of using larger diamond particles to simultaneously improve both the strength and toughness of the tool interface.

(4) The inclination angle of diamond particles exerts a significant non-monotonic influence on interfacial gripping performance. Compared with traditional vertical implantation (0°), inclined implantation at 15°–45° can increase the interfacial strength (peak force) by 200%–300%. This enhancement is due to the introduction of a combined compressive-shear stress state and a mechanical self-locking effect induced by the inclination, which substantially raises the failure threshold. Notably, an inclination of 30° yields the optimal energy-dissipation capacity, indicating a transition in the interfacial failure mode from brittle fracture to ductile slip and plastic ploughing at this angle. Therefore, 45° implantation should be adopted when pursuing ultimate tensile strength, whereas 30° implantation is a better choice for applications involving high-impact loads and requiring enhanced tool toughness.

References

[1] Rossi E, Jamali S, Wittig V, et al. A combined thermo-mechanical drilling technology for deep geothermal and hard rock reservoirs[J]. Geothermics, 2020, 85: 101771.

[2] Wang H, Huang H, Bi W, et al. Deep and ultra-deep oil and gas well drilling technologies: Progress and prospect[J]. Natural Gas Industry B, 2022, 9(2): 141–157.

[3] Guangya Z, Feng M, Yingbo L, et al. Domain and theory-technology progress of global deep oil & gas exploration[J]. Acta Petrolei Sinica, 2015, 36(9): 1156.

[4] Hackley P C, Karlsen A W. Geologic assessment of undiscovered oil and gas resources in Aptian carbonates, onshore northern Gulf of Mexico Basin, United States[J]. Cretaceous Research, 2014, 48: 225–234.

[5] Ma T, Chen P, Zhao J. Overview on vertical and directional drilling technologies for the exploration and exploitation of deep petroleum resources[J]. Geomechanics and Geophysics for Geo-Energy and Geo-Resources, Springer, 2016, 2(4): 365–395.

[6] Guo X, Hu D, Li Y, et al. Theoretical Progress and Key Technologies of Onshore Ultra-Deep Oil/Gas Exploration[J]. Engineering, 2019, 5(3): 458–470.

[7] Tian J, Li J, Cheng W, et al. Working mechanism and rock-breaking characteristics of coring drill bit[J]. Journal of Petroleum Science and Engineering, 2018, 162: 348–357.

[8] Yang Y, Yang Y, Ren H, et al. Research on the working mechanism of the PDC drill bit in compound drilling[J].

Journal of Petroleum Science and Engineering, 2020, 185: 106647.

[9] Kuang Y, Zhang M, Feng M, et al. Simulation and experimental research of PDC bit cutting rock[J]. Journal of Failure Analysis and Prevention, Springer, 2016, 16: 1101–1107.

[10] Kong C, Liang Z, Zhang D. Failure analysis and optimum structure design of PDC cutter[J]. Mechanics, 2017, 23(4): 567–573.

[11] Liao Q, Cui G, Xie T, et al. Study on Different Kinds of Drill Bits and Their Usage in Hard-to-Drill Formations[J]. Chemistry and Technology of Fuels and Oils, Springer, 2023, 59(4): 783–790.

[12] Ersoy A, Waller M D. Wear characteristics of PDC pin and hybrid core bits in rock drilling[J]. Wear, 1995, 188(1): 150–165.

[13] Liu W, Li Y, Gao D. New understandings of the applications of PDC cutters in oil and gas drilling[J]. International Journal of Refractory Metals and Hard Materials, 2024, 122: 106724.

[14] Wang J, Qian D, Sun Y, et al. Surface-set Diamond Bit Design for Deep-Sea Operating Environment of Seafloor Drill and Hole-Bottom Flow Field Analysis[J]. International Journal of Fluid Machinery and Systems, 2022, 15(2): 158–168.

[15] Akün M E, Karpuz C. Drillability studies of surface-set diamond drilling in Zonguldak region sandstones from Turkey[J]. International journal of rock mechanics and mining sciences, Elsevier, 2005, 42(3): 473–479.

[16] [Beaton T, Johnson K. New technology in diamond drill bits improves performance in variable formations[C]//SPE/IADC Drilling Conference and Exhibition. SPE, 2000: SPE-59113-MS.

[17] Lin C-S, Yang Y-L, Lin S-T. Performances of metal-bond diamond tools in grinding alumina[J]. Journal of Materials Processing Technology, 2008, 201(1): 612–617.

[18] Loginov P A, Sidorenko D A, Shvyndina N V, et al. Effect of Ti and TiH2 doping on mechanical and adhesive properties of Fe-Co-Ni binder to diamond in cutting tools[J]. International Journal of Refractory Metals and Hard Materials, 2019, 79: 69–78.

[19] Meiling J, Jiapin C, Zhiyong O, et al. Design & Application of Diamond Bit to Drilling Hard Rock in Deep Borehole[J]. Procedia Engineering, 2014, 73: 134–142.

[20] Chu Z, Guo X, Liu D, et al. Application of pre-alloyed powders for diamond tools by ultrahigh pressure water atomization[J]. Transactions of Nonferrous Metals Society of China, 2016, 26(10): 2665–2671.

[21] Zou Q H, Wang Z G. Experiment on Doping Rare Earth Diamond Tools Matrix Composites with Fe Replacing Co[J]. Applied Mechanics and Materials, 2014, 692: 200–205.

[22] Duan L C, Tang F L, Yang K H, et al. Study of Doping of Rare-Earth Compounds in Iron-Rich Matrix for Diamond Tools[J]. Key Engineering Materials, 2003, 250: 73–77.

[23] Dai Q L, Luo C B, Xu X P, et al. Effects of rare earth and sintering temperature on the transverse rupture strength of Fe-based diamond composites[J]. Journal of Materials Processing Technology, 2002, 129(1–3): 427–430.

[24] Xu X P, Tie X R, Yu Y Q. The effects of rare earth on the fracture properties of different metal–diamond composites[J]. Journal of Materials Processing Technology, 2007, 187–188: 421–424.

[25] Konstanty J. Production parameters and materials selection of powder metallurgy diamond tools[J]. Powder Metallurgy, 2006, 49(4): 299–306.

[26] Liu X F, Li Y Z. The microanalysis of the bonding condition between coated diamond and matrix[J]. International Journal of Refractory Metals and Hard Materials, 2003, 21(3–4): 119–123.

[27] Lu J, Wang Y H, Zang J B, et al. Effect of Si and Ti Coating on Interface Bonding between Diamond and Fe-Based Metal Bond[J]. Key Engineering Materials, 2007, 359–360: 15–18.

[28] Wang Y H, Zang J B, Wang M Z, et al. Properties and applications of Ti-coated diamond grits[J]. Journal of Materials Processing Technology, 2002, 129(1–3): 369–372.

[29] Huang Z, Xiang B, He Y, et al. Thermal residual stress analysis of coated diamond grits[J]. International Journal of Minerals, Metallurgy and Materials, 2009, 16(2): 215–219.

[30] Li L, Chen X, Zhang W, et al. Characterization and formation mechanism of pits on diamond {100} face etched by molten potassium nitrite[J]. International Journal of Refractory Metals and Hard Materials, 2018, 71: 129–134.

[31] Wang J, Wan L, Chen J, et al. Surface patterning of synthetic diamond crystallites using nickel powder[J]. Diamond and Related Materials, 2016, 66: 206–212.

[32] Suh Y S, Joshi S P, Ramesh K T. An enhanced continuum model for size-dependent strengthening and failure of particle-reinforced composites[J]. Acta Materialia, 2009, 57(19): 5848–5861.

[33] Shao J C, Xiao B L, Wang Q Z, et al. An enhanced FEM model for particle size dependent flow strengthening and interface damage in particle reinforced metal matrix composites[J]. Composites Science and Technology, 2011, 71(1): 39–45.

[34] Yuan M N, Yang Y Q, Li C, et al. Numerical analysis of the stress–strain distributions in the particle reinforced metal matrix composite SiC/6064Al[J]. Materials & Design, 2012, 38: 1–6.

[35] Cui W, Wisnom M R. A combined stress-based and fracture-mechanics-based model for predicting delamination in composites[J]. Composites, 1993, 24(6): 467–474.

[36] Alexey S, Gusev A I. Tungsten Carbides: Structure, Properties and Application in Hardmetals[M]. Springer Science & Business Media, Las Vegas, 2013.

[37] Xu J, Sheikh A H, Xu C. 3-D Finite element modelling of diamond pull-out failure in impregnated diamond bits[J]. Diamond and Related Materials, 2017, 71: 1–12.

[38] Machado M, Moreira P, Flores P, et al. Compliant contact force models in multibody dynamics: Evolution of the Hertz contact theory[J]. Mechanism and Machine Theory, 2012, 53: 99–121.